JGR Oceans

RESEARCH ARTICLE
10.1029/2018JC014547

The Role of Ekman Currents, Geostrophy, and Stokes Drift in the Accumulation of Floating Microplastic

Victor Onink[1,2,3], **David Wichmann**[1,4], **Philippe Delandmeter**[1], **and Erik van Sebille**[1]

[1]Institute for Marine and Atmospheric Research, Utrecht University, Utrecht, Netherlands, [2]Climate and Environmental Physics, Physics Institute, University of Bern, Bern, Switzerland, [3]Oeschger Centre for Climate Change Research, University of Bern, Bern, Switzerland, [4]Centre for Complex Systems Studies, Utrecht University, Utrecht, Netherlands

Key Points:
- Ekman currents are the main process behind microplastic accumulation in the subtropical ocean gyres
- Stokes drift contributes to microplastic transport to Arctic regions
- Windage is, on a global scale, not an accurate proxy to model Stokes drift dynamics

Supporting Information:
- Supporting Information S1
- Movie S1
- Movie S2

Correspondence to:
V. Onink,
onink@climate.unibe.ch

Citation:
Onink, V., Wichmann, D., Delandmeter, P., & van Sebille, E. (2019). The role of Ekman currents, geostrophy, and stokes drift in the accumulation of floating microplastic. *Journal of Geophysical Research: Oceans*, *124*. https://doi.org/10.1029/2018JC014547

Received 6 SEP 2018
Accepted 20 FEB 2019
Accepted article online 21 FEB 2019

Abstract Floating microplastic in the oceans is known to accumulate in the subtropical ocean gyres, but unclear is still what causes that accumulation. We investigate the role of various physical processes, such as surface Ekman and geostrophic currents, surface Stokes drift, and mesoscale eddy activity, on the global surface distribution of floating microplastic with Lagrangian particle tracking using GlobCurrent and WaveWatch III reanalysis products. Globally, the locations of microplastic accumulation (accumulation zones) are largely determined by the Ekman currents. Simulations of the North Pacific and North Atlantic show that the locations of the modeled accumulation zones using GlobCurrent Total (Ekman+Geostrophic) currents generally agree with observed microplastic distributions in the North Pacific and with the zonal distribution in the North Atlantic. Geostrophic currents and Stokes drift do not contribute to large-scale microplastic accumulation in the subtropics, but Stokes drift leads to increased microplastic transport to Arctic regions. Since the WaveWatch III Stokes drift and GlobCurrent Ekman current data sets are not independent, combining Stokes drift with the other current components leads to an overestimation of Stokes drift effects and there is therefore a need for independent measurements of the different ocean circulation components. We investigate whether windage would be appropriate as a proxy for Stokes drift but find discrepancies in the modeled direction and magnitude. In the North Pacific, we find that microplastic tends to accumulate in regions of relatively low eddy kinetic energy, indicating low mesoscale eddy activity, but we do not see similar trends in the North Atlantic.

Plain Language Summary Microplastic is a common form of pollution in the oceans, and high floating microplastic concentrations tend to be observed at the surface in the subtropical ocean gyres. These regions are commonly referred to as garbage patches. However, the physical processes that control the buildup in these regions are not yet fully understood. Therefore, we model microplastic transport with various surface current components that correspond to different physical processes. We do this with Lagrangian modeling, where microplastic is represented by virtual particles that are transported by ocean currents. We find good agreement between the modeled distribution with the full surface currents with observations in the North Pacific and North Atlantic and find that the microplastic accumulation is mainly due to the wind-driven Ekman currents. Meanwhile, wave-driven Stokes drift results in microplastic transport to Arctic regions. Since Stokes drift has not consistently been included in microplastic transport modeling, microplastic contamination of Arctic regions might be more severe than currently expected.

1. Introduction

The surface ocean circulation is driven by a large number of processes and is traditionally decomposed into various current components. These include the wind-driven Ekman currents, the geostrophic currents, and wave-induced Stokes drift. It has been shown that the Ekman and geostrophic currents play different roles in marine debris accumulation (Kubota, 1994; Kubota et al., 2005; Martinez et al., 2009), while Stokes drift has been shown to be important for kelp (Fraser et al., 2018) and oil (Drivdal et al., 2014) transport. However, the contribution of Stokes drift using reanalysis data to transport of floating plastic debris has not been studied.

Plastic debris has been found in a large number of marine habitats, such as in the open ocean (Cózar et al., 2014, 2017; Eriksen et al., 2013, 2014; Lebreton et al., 2018), on coastlines (Pieper et al., 2015; Thompson et al., 2004; Young & Elliott, 2016), and on the sea floor (Galgani et al., 2000; Van Cauwenberghe et al., 2013).

The majority of plastic debris found at sea is nonbiodegradable (Duhec et al., 2015; Morét-Ferguson et al., 2010) and can persist for decades in the open ocean (Lebreton et al., 2018), where it can cause harm to marine life through ingestion (Mascarenhas et al., 2004; van Franeker & Law, 2015), entanglement (Henderson, 2001), and by acting as a potential pathway for habitat invasion by alien species (Molnar et al., 2008).

An estimated 4.8–12.7 million tons of plastic entered the ocean in 2010 (Jambeck et al., 2015), and buoyant plastic debris is known to accumulate in the subtropical ocean gyres in each of the ocean basins (Cózar et al., 2014; Eriksen et al., 2014; Law et al., 2014, 2010). For the Pacific basins, this accumulation has been found to be caused by surface Ekman currents (Kubota, 1994; Kubota et al., 2005; Martinez et al., 2009). The geostrophic currents contribute to debris transport but due to their nondivergent nature do not lead to debris accumulation on their own (Martinez et al., 2009). Kubota (1994) found that Stokes drift does not significantly contribute to debris transport, but parametrized Stokes drift as windage with climatological mean wind fields and as such did not take ocean swell into account, which is not locally generated. Windage represents the force of surface wind on exposed portions of an object above the ocean surface, and windage effects have been found to have a significant impact on the trajectories of large objects (Trinanes et al., 2016). For microplastic, windage can play a significant role with low-density plastic such as polystyrene, but for higher density plastics the microplastic particles would be largely below the surface and thus not be exposed to much direct wind stress (Chubarenko et al., 2016).

Comparisons of modeled microplastic distributions with observed microplastic concentrations were done by van Sebille et al. (2015), who modeled the global distribution of microplastic based either on drogued surface drifter trajectories (Maximenko et al., 2012; van Sebille et al., 2012) or using HYCOM/NCODA surface currents (Lebreton et al., 2012) and compared the distributions with observations from surface-trawling plankton nets. It was found that the modeled distributions in the North Pacific closely correlate to spatial patterns in the observations but that in the North Atlantic the agreement of the modeled distributions with observations is weaker. None of the models completely accounted for Stokes drift, which might therefore be a possible explanation for the observed discrepancies.

Processes that act on scales smaller than the mesoscale also play a role in microplastic accumulation. Martinez et al. (2009) found a tendency for debris in the South Pacific to accumulate in regions of relatively low eddy kinetic energy (EKE), which can be considered as a proxy for mesoscale eddy activity (Eden & Böning, 2002). Microplastic concentrations in an anticyclonic eddy have been found to be more than 9 times higher than in a cyclonic eddy (Brach et al., 2018), while resolving mesoscale eddies increases the ability of microplastic to leave accumulation zones in debris simulations (Maes et al., 2016). However, the link between mesoscale eddy activity and plastic debris accumulation in the North Pacific and North Atlantic has not been considered so far.

Since different components of the ocean circulations can change on different time scales, the temporal resolution of ocean circulation data sets can impact modeled transport. Maximenko et al. (2012) reported that temporal variability of the ocean currents has a strong influence of debris transport, as particles do not follow mean ocean current streamlines to reach debris accumulation regions. Particularly transport due to Stokes drift is dependent on the temporal resolution of the data set, since Stokes drift is dependent on the wavefield, which can change on very short time scales by changes in local weather conditions (Bennett & Mulligan, 2017; Montiel et al., 2018).

In this paper we study the contributions of the Ekman and geostrophic currents and Stokes drift on the location of microplastic accumulation zones, that is, quasi-stable regions in the open seas where relatively high microplastic concentrations are observed and which are commonly referred to as garbage patches, on a global scale, with particular focus on the North Pacific and the North Atlantic. This is done by means of Lagrangian simulations with ocean circulation data from reanalysis products (Rio et al., 2015; Tolman, 2009) including surface Ekman and geostrophic currents and surface Stokes drift. The recently proposed Sea surface KInematics Multiscale monitoring satellite (Ardhuin et al., 2018) would be able to measure ocean surface transport components such as Stokes drift directly. Therefore, the role of Stokes drift is of particular interest seeing how its effect on the transport of plastic debris has not been extensively considered (van den Bremer & Breivik, 2018). We also consider how transport is dependent on the temporal resolution of the data sets. Since windage has been used as a proxy for Stokes drift in the past (Breivik & Allen, 2008; Kubota, 1994), we compare the transport due to Stokes drift from the WaveWatch III hindcast (Tolman, 2009) with various windage scenarios to investigate whether windage adequately captures Stokes drift dynamics. The modeled

Table 1
Overview of the Data Sets Used for Particle Advection in the Simulations

Flow field	Data set	Spatial resolution	Temporal resolution	Source
Ekman currents	GlobCurrent v3 Ekman Hs Currents	1/4°	3 hr	Rio et al. (2015)
Geostrophic currents	GlobCurrent v3 Geostrophic Currents	1/4°	24 hr	Rio et al. (2015)
Total currents	GlobCurrent v3 Total Hs Currents	1/4°	3 hr	Rio et al. (2015)
Stokes drift	WaveWatch III Surface Stokes Drift	1/2°	3 hr	Tolman (1997, 2009)
Windage	CFSR surface winds	1/2°	3 hr	Saha et al. (2011)

Note. CFSR = Climate Forecast System Reanalysis.

microplastic distributions in the North Pacific and North Atlantic are compared with observed microplastic concentrations measured with surface-trawling plankton nets from the data set compiled by van Sebille et al. (2015). Finally, we examine the link between mesoscale eddy activity and microplastic accumulation.

2. Materials and Methods

2.1. Ocean Surface Current Data Sets

We use several different reanalysis surface current data sets outlined in Table 1 for the period of 2002–2014. The Ekman and geostrophic flow fields are from the GlobCurrent project (Rio et al., 2015), which combines satellite observations and in situ measurements to obtain estimates of the surface circulation. We will briefly summarize how those currents are derived, but for full details please refer to Rio et al. (2014). Rio et al. (2015) make an initial estimate of the geostrophic currents from altimeter maps and subtract this from surface velocities of ARGO floats to get an estimate of the nongeostrophic velocity of each drifter, which is referred to as the Ekman velocity. The Ekman currents $\vec{u}_{ek}(z)$ are parametrized by Rio et al. (2015) with an amplification factor $\beta(z)$ and Ekman velocity angle $\theta(z)$

$$\vec{u}_{ek}(z) = \beta(z)\vec{\tau}e^{i\theta(z)} \tag{1}$$

This is done by applying a least squares fit between measured Ekman velocities from ARGO drifters and surface wind stress $\vec{\tau}$ data from ERA-Interim (Dee et al., 2011). Based on 841,746 ARGO drifter Ekman velocities, the surface Ekman currents are found by Rio et al. (2015) to be at an angle of $\theta(0) = 30.75°$ to the wind stress (to the right in the Northern Hemisphere, to the left in the Southern Hemisphere), with an amplification factor of $\beta(0) = 0.61 \cdot \mathrm{m^2 \cdot s \cdot kg^{-1}}$. Using 15-m drogued drifters from the Surface Velocity Program, the Ekman current parameters at 15-m depth are $\theta(15\mathrm{m}) = 48.18°$ and $\beta(15\mathrm{m}) = 0.25 \cdot \mathrm{m^2 \cdot s \cdot kg^{-1}}$.

Rio et al. (2015) find the geostrophic velocities of 15-m drogued and undrogued surface drifters from the surface velocity program by subtracting the Ekman velocities from the drifter velocities. Rio et al. (2015) then use the measured geostrophic velocities to update the initial geodetic mean dynamic topography (MDT) to determine the CNES-CLS13 MDT from which the final geostrophic velocities are computed. This incorporation of in situ observations provides missing short-scale information for the boundary currents and equatorial regions that would be missing with just a geodetic approach (Rio et al., 2014). The total surface currents are the sum of the surface geostrophic velocities and the surface Ekman velocities.

The surface Stokes drift is from the WaveWatch III hindcast data set (Tolman, 1997, 2009), where the magnitude and direction of the Stokes drift are based on the wavenumber-direction spectrum (Webb & Fox-Kemper, 2015). The 2002–2014 temporal means of the GlobCurrent and WaveWatch flow fields are shown in Figure 1.

Both the GlobCurrent en WaveWatch III data sets have been compared with drifters and in situ measurements in earlier studies to evaluate the accuracy of the data sets. On scales larger than 100 km, GlobCurrent was found to be able to derive drifter trajectories with good accuracy (Lacorata et al., 2019). However, performance was found to be better in the open ocean than in coastal regions (Cancet et al., 2019; Feng et al., 2018),

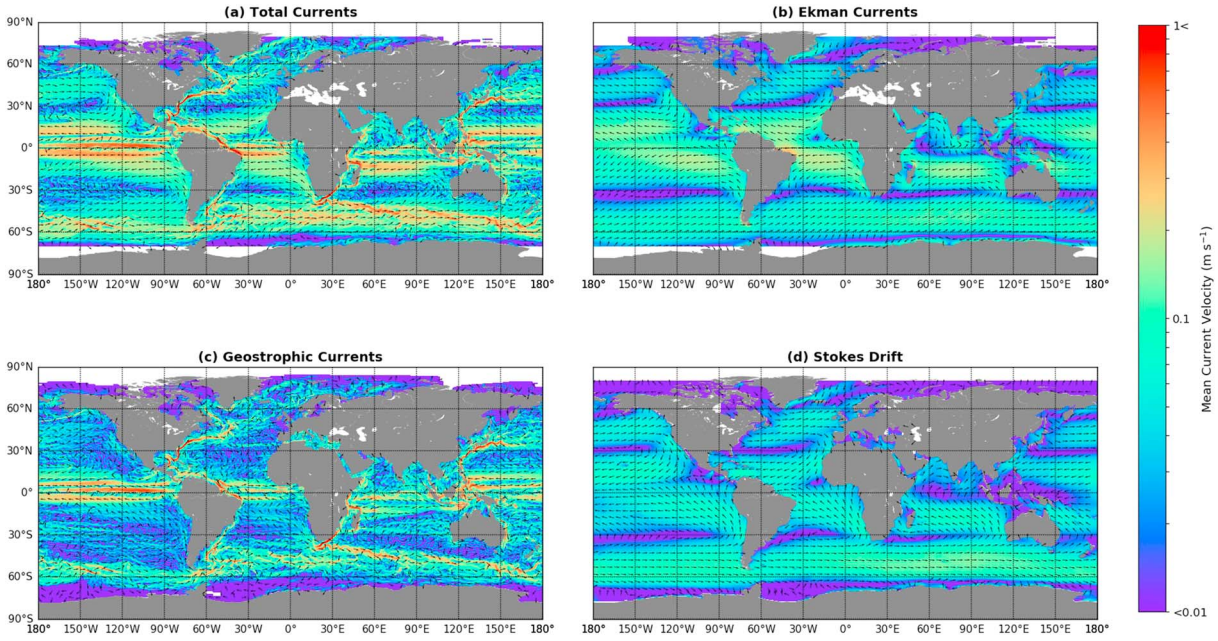

Figure 1. Temporal mean flow fields for the (a) total, (b) Ekman and (c) geostrophic currents, and the (d) Stokes drift. Averages are taken for 2002–2014, with the normalized vectors indicating the mean direction and the color map indicating the current magnitude. Note that the velocity scale is logarithmic.

with the spatial resolution being too coarse and the MDT insufficiently resolved in coastal regions to yield accurate estimates of coastal currents. The GlobCurrent total currents have been found to underestimate current strengths, although the extent to which this occurs depends on the region being considered (Cancet et al., 2019; Hart-Davis et al., 2018). Comparison of the WaveWatch III Stokes drift data sets with in situ measurements from drifters showed high correlations (Rascle & Ardhuin, 2013; Tamura et al., 2012), with root-mean-square errors on the order of several centimeters per second (Tamura et al., 2012).

It must be noted that the GlobCurrent and WaveWatch III data sets are not independent. The parametrization of the GlobCurrent Ekman currents does not fully remove effects due to Stokes drift, and so summation of the flow fields will lead to an overestimation of the Stokes drift effect. Additionally, both data sets do not capture subgrid scale dispersion, which can influence the distribution of microplastic (Maes et al., 2016).

2.2. Windage Proxy

Windage effects are dependent on the object size, shape, and buoyancy, and the coupling strength between the local wind and the resultant windage velocity of the object is highly variable (Chubarenko et al., 2016). Increased buoyancy and size result in higher freeboard, which increases the exposure of the object to the surface winds and therefore stronger windage effects. We use the windage classification described by Duhec et al. (2015), which classifies debris as either low windage (e.g., fishing nets and small plastic fragments), medium windage (e.g., polystyrene and partially filled PET bottles), or high windage (e.g., unfilled PET bottles and fishing buoys). We compare the Stokes drift with each of these windage scenarios, where the windage is 1%, 3%, or 5% of the local wind vector, to investigate which would be most appropriate as a proxy for Stokes drift. We use the CFSR (Saha et al., 2011) wind fields for 2002–2014 (Table 1), which is the same wind field used for the WaveWatch III hindcast (Tolman, 2009).

2.3. Microplastic Observation Data Set

The data set of microplastic measurements taken by surface-trawling plankton nets was compiled by van Sebille et al. (2015). A total of 11,632 trawl measurements taken between 1979 and 2013 was considered by van Sebille et al. (2015), of which 6,812 were collected in the North Atlantic, 2,551 were collected in the North Pacific, and the rest were spread out over the Southern Hemisphere and in the Mediterranean. While microplastic commonly refers to plastic debris <5 mm, van Sebille et al. (2015) refer to any plastic debris collected with a plankton net trawl as microplastic, as most of the plastic collected in plankton net trawls are small fragments. We use the same definition in all following references to microplastic.

Given that the samples were collected over a period of 34 years and that microplastic concentrations are sensitive to the vertical mixing due to surface wind stress (Kukulka et al., 2012), van Sebille et al. (2015) corrected for the sampling year and the variable wind conditions. All concentrations are ultimately expressed in terms of counts square kilometer and are binned into 1° bins. Given that the observational record for the Southern Hemisphere is very limited, it is not possible to make meaningful comparisons between modeled microplastic distributions and observations for these regions. We therefore focus on the North Atlantic and the North Pacific.

2.4. Lagrangian Transport

We use Parcels (Probably A Really Computationally Efficient Lagrangian Simulator; Lange & Van Sebille, 2017 to model microplastic as virtual particles which are advected using ocean flow field data. A change in the position $\vec{x}$ of a particle is computed by

$$\vec{x}(t+\Delta t) = \vec{x}(t) + \int_{t}^{t+\Delta t} \vec{v}(\vec{x}(\tau),\tau)\mathrm{d}\tau \tag{2}$$

where $\vec{v}(\vec{x}(t),t)$ is the flow velocity at the particle location $\vec{x}(t)$ at time t. The flow velocity $\vec{v}(\vec{x}(t),t)$ at the particle location is obtained through linear interpolation of the flow field data in space and time and depending on the simulation the flow velocity consists of

$$\vec{v} = \begin{cases} \vec{v}_{\mathrm{tot}} = \vec{v}_{\mathrm{ek}} + \vec{v}_{\mathrm{geo}}, & \text{Total currents simulation} \\ \vec{v}_{\mathrm{ek}}, & \text{Ekman currents simulation} \\ \vec{v}_{\mathrm{geo}}, & \text{Geostrophic currents simulation} \\ \vec{v}_{\mathrm{sd}}, & \text{Stokes drift simulation} \\ \vec{v}_{\mathrm{tot}} + \vec{v}_{\mathrm{sd}}, & \text{Total currents + Stokes drift simulation} \end{cases} \tag{3}$$

where $\vec{v}_{\mathrm{tot}}$, $\vec{v}_{\mathrm{ek}}$, $\vec{v}_{\mathrm{geo}}$, and $\vec{v}_{\mathrm{sd}}$ are total currents, Ekman currents, geostrophic currents, and Stokes drift, respectively. Equation (2) is integrated with a fourth-order Runge-Kutta scheme with an integration time step of 30 min.

All simulations are carried out for 2002–2014. Since the geostrophic current data set has a temporal resolution of 1 day, we use daily mean fields for the total currents, Ekman currents, Stokes drift, and wind fields for consistency with the temporal resolution. We also carry out simulations with 3-hourly data to study the effect of current variations on subdaily time scales.

For the initial microplastic distribution, we use a homogeneous distribution with particles placed at 1° intervals for the global simulations (34,515 particles). We also run separate simulations for the North Pacific and North Atlantic starting from a homogeneous distribution with particles placed at 1/2° intervals (30,091 particles for the North Pacific and 18,632 particles for the North Atlantic), to allow better comparisons of the modeled distributions with observations. The majority of marine plastic debris is thought to enter the oceans from the coastlines from rivers (Lebreton et al., 2017), direct littering at the coast (Jambeck et al., 2015) or as runoff from natural disasters (Prasetya et al., 2011). However, the input distribution remains highly uncertain (Lebreton et al., 2017). The input distribution is important for modeled concentrations. However, since the purpose of this study is to determine the processes determining the average spatial locations of the accumulation zones, indicated by the spatial location of the peak microplastic concentration, it was assumed that the effect of the initial distribution is small. This is supported for the long-term distribution by the close agreement between the accumulation zone locations modeled by Maximenko et al. (2012; which started with particles with a initially homogeneous distribution) and those modeled by van Sebille et al. (2012) and Lebreton et al. (2012; which released particles at the coasts scaled according to coastal population densities). The reported modeled concentrations are averaged over the final year of the 12-year simulation and binned into 1° bins to determine the average locations of the accumulation zones.

The GlobCurrent data sets resolve some mesoscale eddies, and EKE is taken as a proxy for mesoscale eddy activity. Each particle samples the local EKE along its trajectory, where the EKE is computed from the total surface current anomaly components u' and v', which are computed with respect to the time-averaged total surface currents for 2002–2014 according to Reynolds decomposition. These current anomalies are due to both mesoscale eddies and meandering of or seasonal variations in the surface currents. The EKE is computed according to

$$\mathrm{EKE} = \frac{(u')^2 + (v')^2}{2} \tag{4}$$

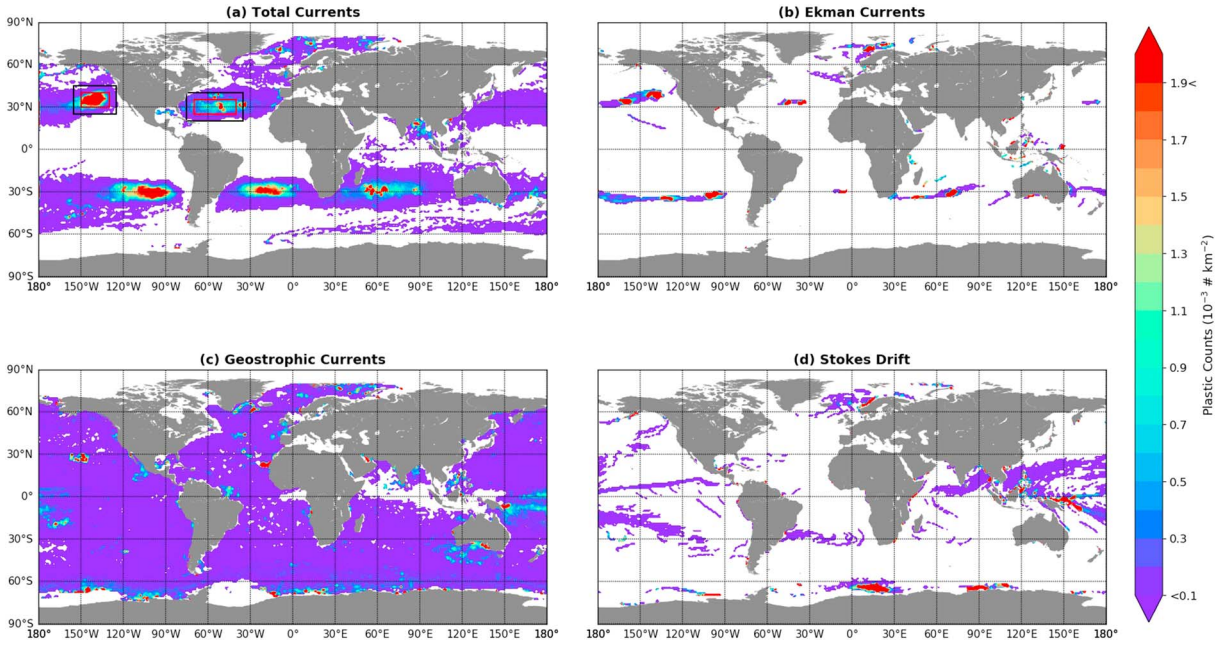

Figure 2. The average particle density of the final year of the global Lagrangian runs with the virtual particles advected by the daily mean (a) total, (b) Ekman and (c) geostrophic currents, and the (d) Stokes drift. The red and black boxes in the North Pacific and North Atlantic in panel (a) indicate the accumulation zone and extended accumulation zone for that basin used in the eddy kinetic energy analysis.

Preliminary simulations showed that almost half the particles beached over the course of a 12-year simulation, which occurs when particles are advected onto a land cell. However, this is likely at least partly due to the coastal currents not being properly resolved in the GlobCurrent and WaveWatch III data sets. Since the purpose of this study does not involve investigating particle beaching, we implement an artificial shore-normal boundary current with a velocity of 1 m/s that is nonzero only at the coast. This prevents the beaching of particles and allowed for more robust statistics, although a number of particles would still get trapped very near to the coastlines if the flow field was consistently directed landward. The antibeaching current is not found to influence the microplastic distribution in the subtropical open ocean, but it can lead to local differences in coastal regions (Figure S1 in the supporting information).

3. Results

3.1. Global

Simulations with the total currents show the formation of accumulation zones in each of the subtropical ocean gyres (Figure 2a), as well as parts of the Arctic between Greenland and Norway, which agrees with observations (Cózar et al., 2014, 2017; Eriksen et al., 2014). The distributions are found to be quasi-stationary over the final 4 years of the simulation (Figure S2). The accumulation zone with the most particles is in the South Pacific, but this is an artifact of the large number of particles within the basin at the beginning of the simulation, as was similarly stated by Maximenko et al. (2012). The location of the accumulation zones is due to the Ekman currents (Figure 2b), with the locations of the Ekman current accumulation zones matching those of the total current accumulation zones. However, the Ekman currents on their own generally lead smaller accumulation zones than the total currents, which is due to geostrophic currents. The geostrophic currents counter microplastic accumulation in the subtropics and disperse the microplastic over a larger surface area. On their own, the geostrophic currents lead to elevated concentrations in the open ocean north of Brazil and east of New Guinea (Figure 2c). However, this is likely a product of the geostrophic current data set, as the equatorial region has the highest estimated error of the geostrophic currents relative to observations (Rio et al., 2015). There is also accumulation in the North Pacific northeast of Hawaii. However, this is due to a small cluster of particles being trapped by local currents and not large numbers of particles transported to the accumulation zone by the large-scale circulation as with the total current simulation (Movied S1 and S2). Similar regions of temporary high concentrations in the open ocean with the geostrophic currents are also visible south of Iceland (Figure S3).

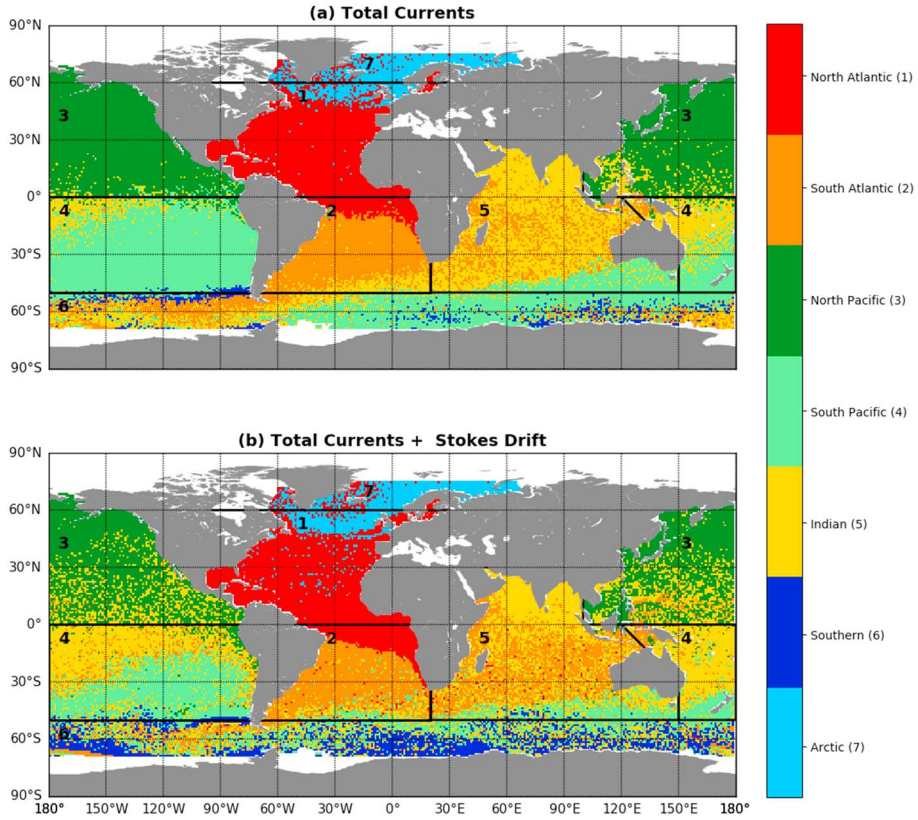

Figure 3. Connectivity of the ocean basins based on virtual particles advected with daily mean (a) total currents and the (b) sum of the daily mean total currents and Stokes drift. Particles are shown at their initial position colored according to their position at the end of the simulation. The coloring is based on the black boxes.

In the Pacific basins, Stokes drift largely clears the subtropical gyres of microplastic, transporting it west toward New Guinea (Figure 2d). Microplastic is found in the subtropical ocean gyre in the South Atlantic but with low concentrations relative to accumulation zone concentrations in the total current simulation. Outside the equatorial regions, the highest concentrations are found near Antarctica and north of Norway, indicating that Stokes drift on its own leads to poleward microplastic transport.

The influence of Stokes drift in combination with the Ekman and geostrophic currents is apparent by comparing the connectivity of the ocean basins when particles are advected solely by total currents or by the sum of total currents and Stokes drift (Figure 3). Tracking the initially uniformly distributed particles indicates connections between the different ocean basins over a 12-year period, which show that the ocean basins do not follow strict cartographic boundaries. This is especially the case for the Southern Hemisphere (Figure 3a), where the basins stretch westward in bands in the simulation with total currents (Froyland et al., 2014). Only around half of all particles within the South Pacific, South Atlantic, and Indian basins end within the same basin they originated from, compared to 96.0% and 82.0% for the North Pacific and North Atlantic (Table 2).

Since the WaveWatch and GlobCurrent data sets are not independent, the addition of Stokes drift to the total currents can lead to an overestimation of the Stokes drift effects. However, it gives a first indication of the effects of Stokes drift relative to the other current components. Stokes drift has a strong influence on the interbasin connections, particularly in the Southern Hemisphere (Figure 3b). The South Pacific has the greatest reduction in particle number from 26.6% of the total particles to 15.8%, with the majority of these particles going either to the South Atlantic or the Indian basin. The increased connectivity with the North and South Pacific leads to a large increase in the number of particles in the Indian basin, which rises from 20.4% of the total particles to 27.4% (Table 2). This transport compensates for the increased connectivity between the South Atlantic and Indian basins, indicated by the share of particles in the South Atlantic that originate from the Indian basin rising from 28.2% to 39.6%.

Table 2
The Total Number of Particles Within Each Basin (According to the Definitions in Figure 3), at the End of the Global Simulations, With Particles Advected by Either Daily Mean Total Currents or the Sum of the Daily Mean Total Currents and Stokes Drift

	North Pacific		South Pacific		North Atlantic		South Atlantic	
Basin of origin	Total	Total + Stokes	Total	Total + Stokes	Total	Total + Stokes	Total	Total + Stokes
North Pacific	96.0%	93.4%	0.9%	0.0%	0.0%	0.0%	0.4%	3.3%
South Pacific	3.2%	5.1%	55.3%	46.6%	0.0%	0.0%	0.7%	9.2%
North Atlantic	0.0%	0.0%	0.0%	0.0%	82.0%	75.2%	0.0%	0.0%
South Atlantic	0.0%	0.1%	0.2%	3.5%	13.5%	17.2%	44.9%	34.3%
Indian	0.8%	1.0%	8.9%	12.6%	0.1%	2.0%	28.2%	39.6%
Southern	0.0%	0.4%	34.7%	37.3%	0.0%	0.4%	25.8%	13.6%
Arctic	0.0%	0.0%	0.0%	0.0%	4.4%	5.2%	0.0%	0.0%
Total Particles	7,146	5,809	9,178	5,452	4,097	4,205	4,942	5,603

	Indian		Southern		Arctic	
Basin of origin	Total	Total + Stokes	Total	Total + Stokes	Total	Total + Stokes
North Pacific	6.5%	19.2%	0.0%	0.0%	0.0%	0.0%
South Pacific	18.1%	34.3%	5.0%	2.5%	0.0%	0.0%
North Atlantic	0.0%	0.0%	0.0%	0.0%	38.8%	48.3%
South Atlantic	5.3%	3.4%	0.0%	0.2%	0.7%	0.0%
Indian	50.1%	28.6%	0.0%	1.8%	0.0%	0.0%
Southern	20.0%	14.5%	95.0%	95.5%	0.0%	0.0%
Arctic	0.0%	0.0%	0.0%	0.0%	60.5%	51.7%
Total particles	7,028	9,446	818	2,557	1,260	1,405

Note. The left column indicates the basin of origin. Percentages indicate the fraction of total particles in the final basin that originate from the given basin of origin.

The poleward transport due to Stokes drift, shown in Figure 2, is apparent by the 213% increase in the total number of particles in the Southern basin at the end of the simulation relative to the simulation with just the total currents. However, this increase is largely due to particles starting in the Southern basin being retained, although there are also slight increases in the number of particles reaching the Southern basin from the Indian, South Atlantic, and South Pacific basins. Meanwhile, there is also a slight increase of particles in the Arctic basin. This is due to increased poleward transport from the North Atlantic, which is apparent from the share of particles in the Arctic region that originate in the North Atlantic increasing from 38.8% to 48.3%.

Finally, the inclusion of Stokes drift increases cross-equatorial particle transport. With just the total currents, only 0.4% of particles in the South Atlantic originate from the North Pacific, while in the Indian basin the North Pacific share is 6.5%. This, respectively, rises to 3.3% and 19.2% with Stokes drift included. No particles from the North Atlantic are within the Southern Hemisphere at the end of the simulation.

3.2. Comparison With Observations

We focus on the North Pacific and North Atlantic for the comparison of simulated distributions with observations as these are the only regions with a sufficient sampling density.

The North Pacific accumulation zone with the total currents shows good agreement with observations, with peaks in the meridional and zonal means of the microplastic concentration closely agreeing at (35°N, 140°W; Figures 4a and 4b). In the North Atlantic the model correctly predicts accumulation in the subtropics (Figure 4c). However, while the observational record has a pronounced peak in the meridional mean microplastic concentration at 40°W, the elevated concentrations in the total currents simulation are spread over 75°to 30°W, with only small peaks at 34°W and 50°W to 55°W (Figure 4d). We also observe high concentrations in the Arctic at around 70°N.

The zonal and meridional means of the geostrophic current simulation distribution show that in the North Pacific there is a slight peak in the subtropics at 26°N and 30°N (Figure 4a). However, the concentrations are much lower than with the total currents, which suggests that these are only small, local areas of microplastic

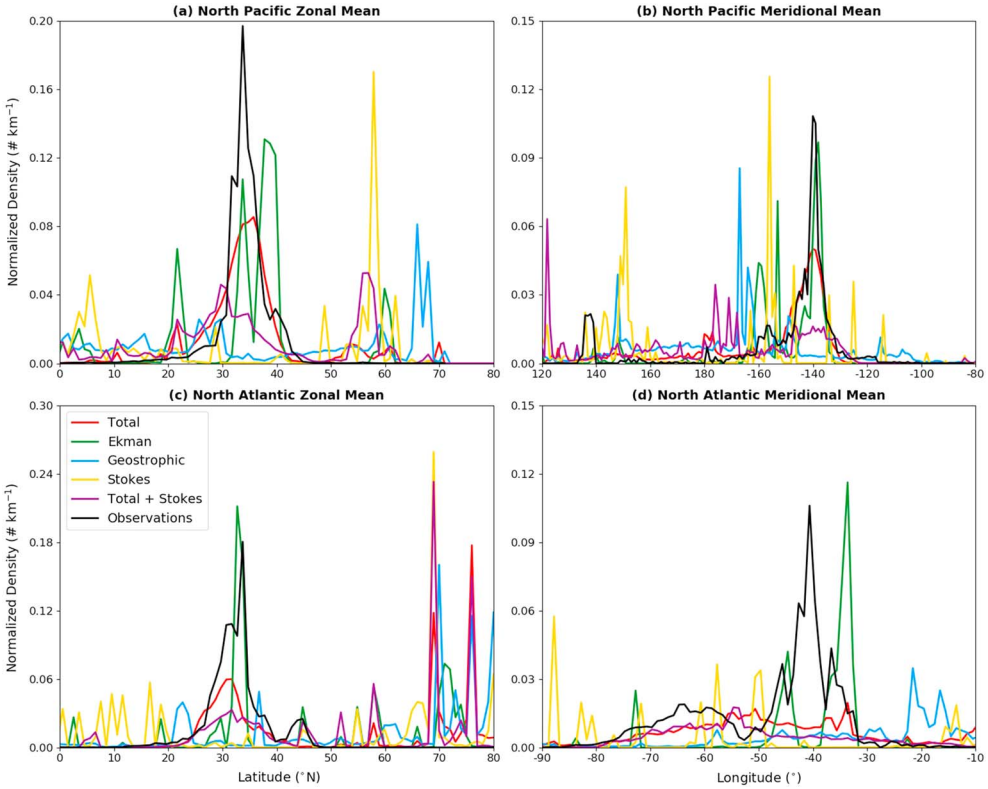

Figure 4. Normalized zonal and meridional spatial means of observed (van Sebille et al., 2015) and modeled microplastic concentrations with various daily mean surface current components for the North Pacific and North Atlantic simulations. (a, b) For the North Pacific the means are computed for the region of 0°N to 80°N and 120°E to 80°W. (c, d) In the North Atlantic the means computed are for the region 0°N to 80°N and 90°W to 60°E. All zonal and meridional distributions are normalized separately such that the integrated area under each curve is equal to 1.

accumulation (Movie S1). There are no elevated concentrations in the subtropics in the North Atlantic (Figure 4c), with the only peaks in concentration being due to particles getting stuck near coastlines, especially in Arctic regions. In contrast, the Ekman currents do lead to strong peaks in concentration in the subtropics, with the location of the concentration peaks in the North Pacific closely agreeing with the concentration peaks in the observations (Figures 4a and 4b). There is only a small shift in the position of the concentration peak relative to the concentration peak in the total current distribution, indicating that geostrophic currents have little impact on the location of maximum accumulation. We do observe that the total current simulations show much lower concentrations than the Ekman current simulations, which is due to the strong dispersion of microplastic by the geostrophic currents being included in the total currents simulation (Figure 2c).

In the North Atlantic the Ekman currents lead to the formation of two subtropical microplastic concentration peaks at 35°W and 45°W (Figure 4d). The peaks are within 5° east and west of the meridional concentration peak in the observations at 40°W, but clear bimodal peaks are not visible in the observation record. The addition of geostrophic currents spreads out the microplastic, and the westernmost peak is found at 50–55°W. The location of easternmost peak is unaffected, but the concentrations are lowered by a factor of 5.

The addition of the Stokes drift to the total currents does not lead to closer agreement between observed and modeled microplastic distributions (Figure 4) due to the overestimation of Stokes drift. In the North Pacific the addition of Stokes drift causes much greater temporal variance in the location of the accumulation zone, leading to a less defined accumulation zone as the temporal averaging spreads out the peak concentrations over a larger area. The peak concentration in the zonal direction has shifted further south relative to observations, while there is no clear peak at all in the meridional direction (Figures 4a and 4b). In the North Atlantic the general shape of the microplastic distribution is unchanged in the zonal and

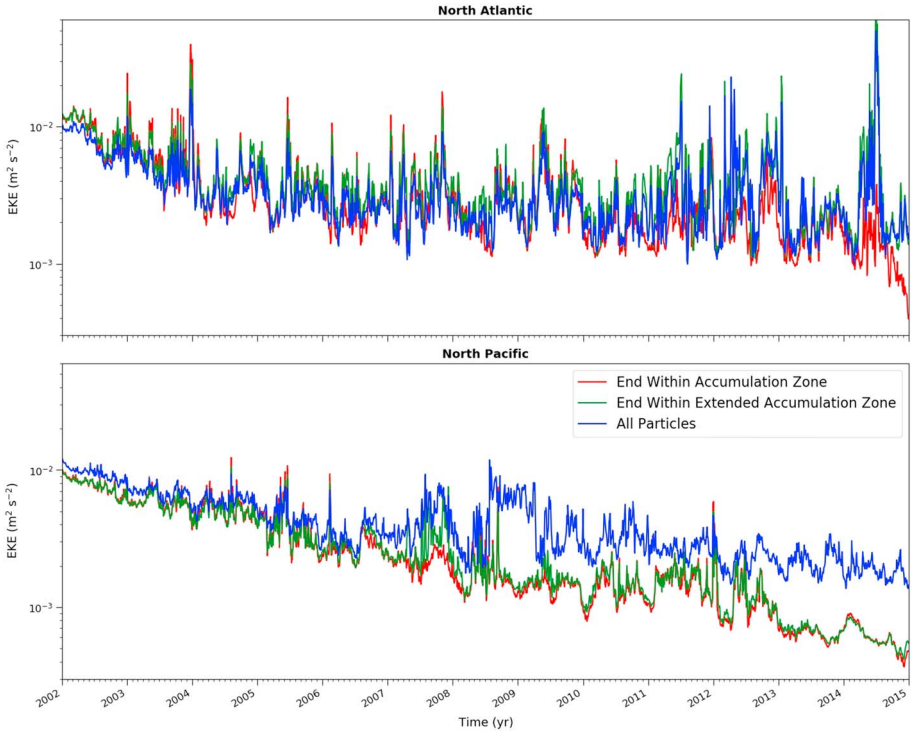

Figure 5. Average eddy kinetic energy over time of particles that end within the accumulation zone, of particles that end within the extended accumulation zone, and of all particles within the North Pacific and North Atlantic simulations. The particles are advected with daily mean total currents. The North Atlantic accumulation zone is defined as 25°N to 35°N and 40°W to 70°W, while the extended North Atlantic accumulation zone is defined as 20°N to 40°N and 35°W to 75°W. The North Pacific accumulation zone is defined as 30°N to 40°N and 130°W to 150°W, while the extended North Pacific accumulation zone is defined as 25°N to 45°N and 125°W to 155°W, as shown in Figure 2a. Please note that the eddy kinetic energy axis is logarithmic.

meridional directions, but the concentrations are consistently lower (Figures 4c and 4d). We do observe higher concentrations in the Arctic regions, which suggest that the reduced concentrations in the subtropics are due to increased transport northward.

3.3. Role of Mesoscale Eddy Activity

For the North Pacific and North Atlantic total current simulations, time series of the average EKE are computed for all particles within the basins and for all particles whose final position at the end of the simulations is within the respective accumulation zones. The accumulation zones are selected such that they encompass the elevated microplastic concentrations in the subtropical ocean gyre, as shown in Figure 2a. The extended accumulation zones shift the accumulation zone boundaries by 5° in each cardinal direction.

In the North Pacific the average EKE for particles in the accumulation zone at the end of the simulation is consistently lower than the average for all particles (Figure 5a), which at the end of the simulation has grown by an order of magnitude. This is unchanged by considering the extended North Pacific patch. The time series of the extended accumulation zone shows a similar trend and indicates that observed trend is not just a product of the selected accumulation zone boundaries. Microplastic in the North Pacific therefore appears to accumulate in a region of relatively low mesoscale eddy activity, as was also reported for the South Pacific (Martinez et al., 2009).

The North Atlantic average EKE time series for all particles and just the accumulation zone particles do not show a strong correlation (Pearson $r = 0.560$, $p < 0.01$), and the average EKE for the accumulation zone particles is not consistently lower than the particles in the North Atlantic as a whole (Figure 5b). There is a drop in the average EKE at the end of the simulation, but this is a product of the selected accumulation zone boundaries as this drop is not visible when considering the extended North Atlantic accumulation zone. There is therefore no indication that microplastic in the North Atlantic tends to accumulate in regions of relatively low mesoscale eddy activity.

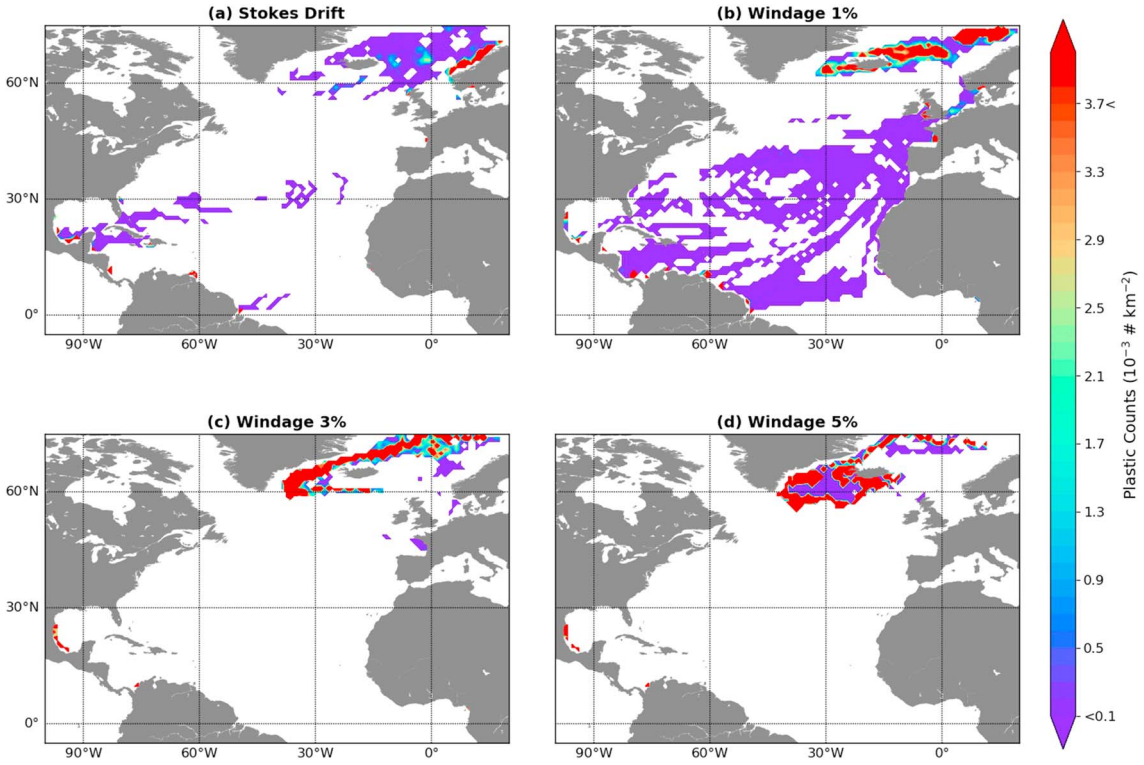

Figure 6. The average particle density of the final year of North Atlantic Lagrangian simulations with the virtual particles advected by daily mean (a) Stokes drift and (b) 1%, (c) 3%, and (d) 5% windage from daily mean CFSR wind fields. CFSR = Climate Forecast System Reanalysis.

3.4. Comparison of Windage With Stokes Drift

In the North Atlantic, particle advection in the two higher windage scenarios leads to particle distributions that are similar to the distribution from advection by Stokes drift in that particles are largely cleared from the subtropical open ocean in the higher windage scenarios (Figure 6). Furthermore, we see most accumulation in the Carribbean or between Greenland and Norway. However, with Stokes drift particles in the Arctic regions are largely driven toward the coast, while within the windage scenarios more particles tend to remain in the open ocean. Additionally, in the 1% windage scenario more particles remain in the subtropics than with Stokes drift. The high concentrations in the Arctic regions with each of the windage scenarios do not indicate a stable accumulation zone but are due to high numbers of particles passing through the region in the final simulation year.

All windage scenarios result in the same general microplastic distribution, but the 3% and 5% windage scenarios result in particle velocities that are much higher than Stokes drift. The global average root-mean-square errors of the 3% and 5% windage scenario Eulerian velocity fields relative to the Stokes drift Eulerian velocity fields are 0.282 and 0.225 m/s, while for the 1% windage scenario Eulerian velocity fields the global average RMSE is only 0.033 m/s. The RMSE is not globally uniform, with the smallest RMSE in the equatorial regions and the highest RMSE at 30–60° latitude and in the polar regions (Figure 7). The higher latitudes correspond to regions with a large amount of ocean swell, which have little correlation with local wind conditions (Fan et al., 2014).

Considering the zonal and meridional velocity components of the Stokes drift and windage separately, there is a closer correlation between the zonal velocity components than the meridional components (Figure 8). With the zonal velocity, the coefficient of determination (r^2) for most of the open ocean is 0.8 or higher, with lower coefficients only being found in the polar and select equatorial regions. The poor correlations around the equator are likely due to the weak winds in this region, with small fluctuations around 0 m/s leading to poor correlations, even if the RMSE is small (Figure 7). The poor correlations in the polar regions are likely due to the presence of sea ice. In comparison, the coefficients of determination for the meridional velocity components are consistently lower, most likely due to Stokes drift being predominantly zonal (Figure 1d).

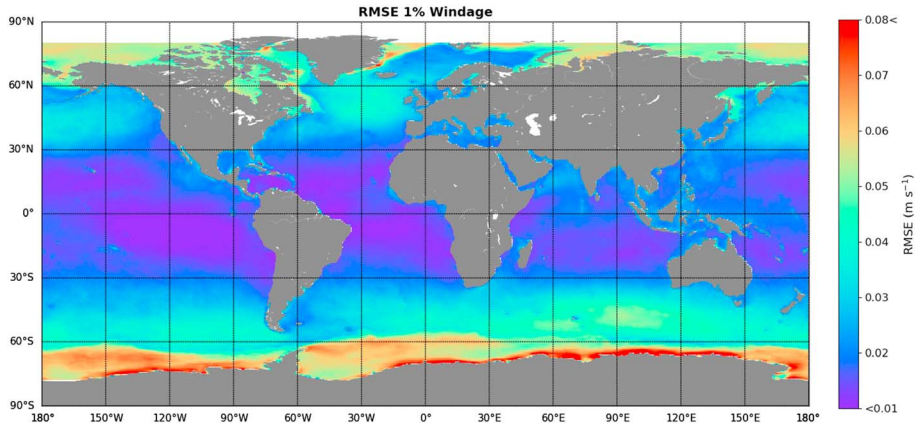

Figure 7. Root-mean-square error (RMSE) between the speed of the Stokes drift and the 1% Windage scenario. The RMSE is computed on a 0.5° × 0.5° grid for 1 January 2002 to 31 December 2014.

This has implications for the direction of the windage, for low correlation for either velocity component, results in the direction of the windage Eulerian velocity field deviating from the direction of the Stokes drift Eulerian velocity field.

3.5. Impact of Temporal Resolution of Flow Fields

Simulations of the North Atlantic where particles are advected using flow field data sets with a temporal resolution of 3 hr show that the higher temporal resolution of the total currents does not have a strong impact on the modeled accumulation zone (Figures 9a and 9c). The peak concentrations remain in the same location, although the zonal spread of microplastic is smaller when using the higher temporal resolution

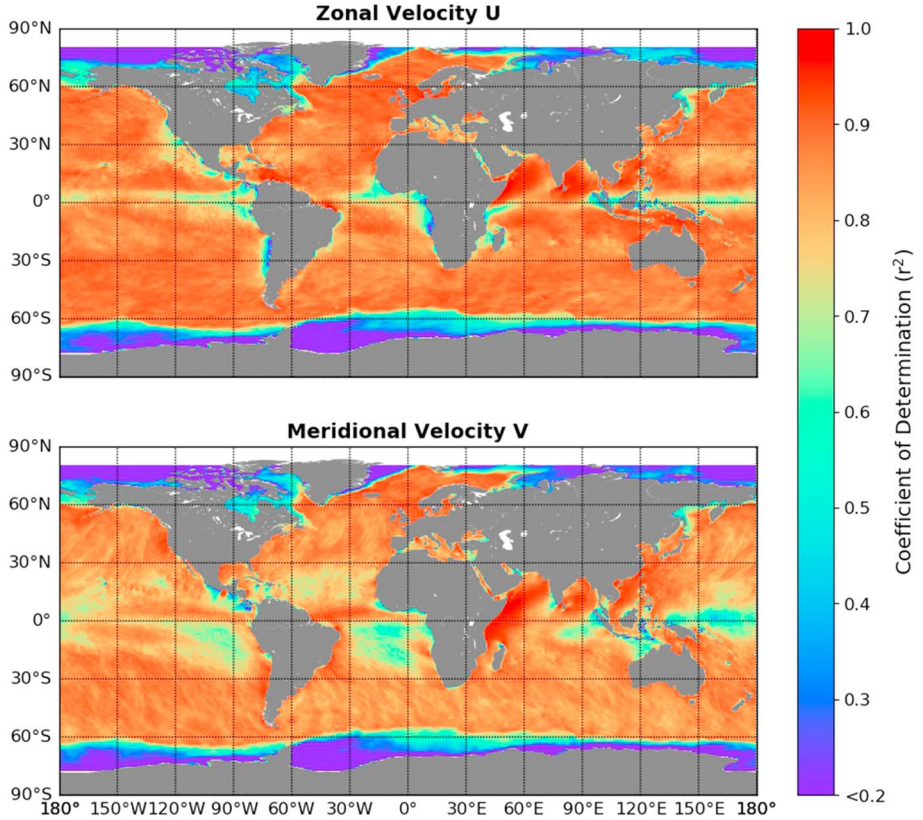

Figure 8. Coefficient of determination r^2 for the zonal and meridional velocity components of Stokes drift and windage. Coefficients are computed on a 0.5° ×0.5° grid for 1 January 2002 to 31 December 2014.

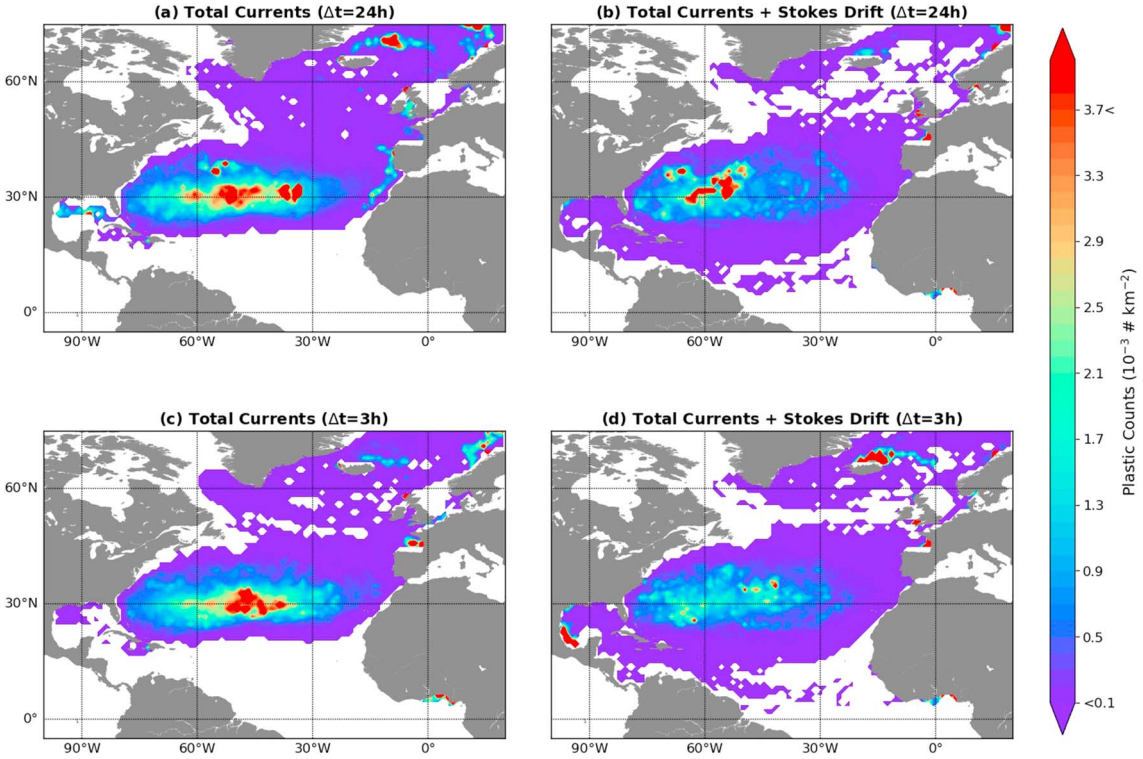

Figure 9. The average particle density of the final year of North Atlantic Lagrangian simulations with the virtual particles advected by (a, c) total currents or (b, d) the sum of the total currents and Stokes drift. The flow field data sets have a temporal resolution of either $\Delta t = 24$ hours or $\Delta t = 3$ hours.

data set. In the case of the North Pacific the resultant microplastic distribution is similarly largely unaffected by the change in temporal resolution of the total current data set (Figures 10a and 10c).

The effect of the increased temporal resolution of the microplastic distribution is more apparent with the sum of the total currents and Stokes drift. In the North Atlantic there is no clear peak in microplastic concentrations in the subtropics, as is the case when considering the daily mean flow field scenario (Figures 9b and 9d). There is also more microplastic in the Arctic regions, with high concentrations north of Iceland that are not visible with the lower temporal resolution. In the case of the North Pacific, the inclusion of Stokes drift with the daily mean data sets already results in there being no clear accumulation zone in the subtropics and increasing the temporal resolution does not change this (Figures 10b and 10d).

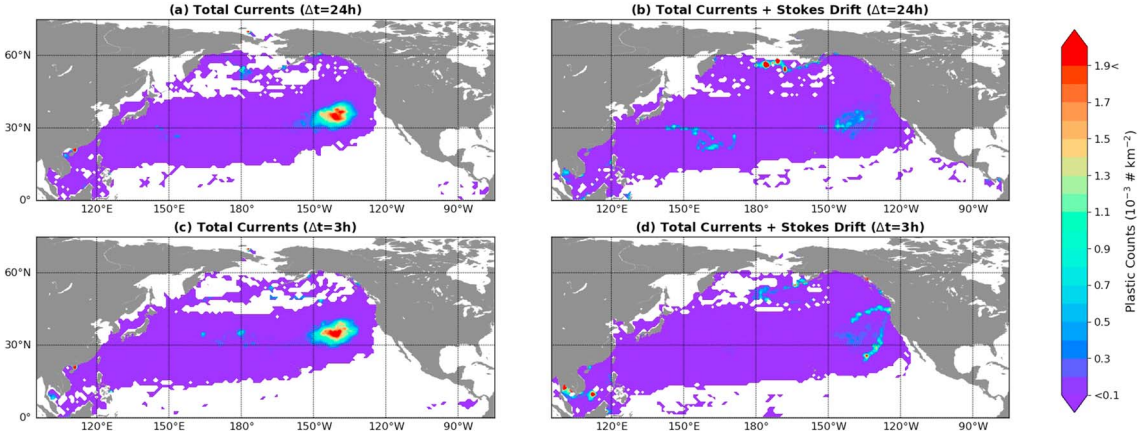

Figure 10. The average particle density of the final year of North Pacific Lagrangian simulations with the virtual particles advected by (a, c) total currents or (b, d) the sum of the total currents and Stokes drift. The flow field data sets have a temporal resolution of either $\Delta t = 24$ hr or $\Delta t = 3$ hr.

4. Discussion and Conclusions

In this study we investigate the role of various surface current components on the accumulation of microplastic in the subtropical ocean gyres. This is done by Lagrangian particle tracking with ocean circulation data from reanalysis products. The modeled zonal and meridional microplastic distributions with the total currents in the North Pacific, and zonally in the North Atlantic, show good agreement with the observational microplastic distributions. The location of the accumulation zones is largely determined by the Ekman currents, but the geostrophic currents have a strong influence on the shape of the microplastic distribution. This agrees with earlier work on the Pacific basins by Kubota (1994), Kubota et al. (2005), and Martinez et al. (2009), which found Ekman current to lead to debris transport to the subtropics, where geostrophic currents transport the debris eastward. In our simulations we find the Ekman currents able to account for the eastward transport on their own. This is due to the angle of the surface Ekman currents to the surface wind stress being 30.75° instead of 45° as predicted by Ekman theory and used by Kubota (1994), Kubota et al. (2005), and Martinez et al. (2009). In the subtropics this leads to a stronger zonal velocity component and therefore more zonal microplastic transport. Considering the close agreement with observations, especially in the North Pacific, the GlobCurrent parametrization of the Ekman currents based on ARGO float Ekman velocities is likely a better indicator of the real surface ocean circulation than Ekman currents computed solely based on Ekman theory. This does assume that floating microplastic concentrations are an accurate tracer of the real surface circulation.

Stokes drift has not been consistently considered in all global microplastic transport simulations, and this can lead to an underestimation of the microplastic contamination of Arctic regions. Our simulations showed that Stokes drift on its own does not contribute to microplastic accumulation in the subtropics, but we do observe high concentrations near Antarctica and Norway. In combination with the total currents, Stokes drift leads to more microplastic particles in the Arctic and Southern Oceans. While in the Arctic this is due to increased transport from the North Atlantic, in the Southern Ocean the increase is largely due to retention of particles intially already in the Southern Ocean due to the uniform start distribution. Fraser et al. (2018) showed that Stokes drift can lead to kelp crossing the strong circumpolar winds and currents to reach the Antarctic coast, but it remains unclear whether this is also the case for microplastic.

Unfortunately, it is currently not possible to accurately determine the combined effect of the total and Stoke currents from reanalysis flow fields alone. The GlobCurrent and WaveWatch III data sets are not independent, and the sum of total currents and Stokes drift leads to overestimation of Stokes drift effects. The GlobCurrent surface Ekman currents are parametrized based on the nongeostrophic velocities of ARGO drifters, and these drifter velocities contain a Stokes drift component (Rio et al., 2014). However, the parametrization of the Ekman currents is based on the local surface wind stress and therefore does not properly account for the contribution of ocean swell to Stokes drift. This is shown by our comparison of Stokes drift with the windage scenarios, where regions with high amounts of ocean swell show a higher RMSE between the Eulerian velocity fields of Stokes drift and the 1% windage scenario. We also see that the windage direction does not always agree with the direction of Stokes drift, which can have important implications for transport modeling. This is especially the case for polar regions, which are most affected by transport due to Stokes drift but where we also see the greatest discrepancy between Stokes drift and windage scenarios.

There is a need for instruments capable of direct global measurements of Stokes drift in the open ocean. This would provide a global observation data set of Stokes drift, which in turn can be used to correct for Stokes drift in the parametrization of Ekman currents. In this manner, summation of all current components would be possible and further analysis of the contribution of Stokes drift to microplastic transport would be possible. The recently proposed Sea surface KInematics Multiscale satellite would use near-nadir Ka-band Doppler radar with incidence angles of 6° and 12° to measure the directional wave spectrum, from which the Stokes drift can be derived (Ardhuin et al., 2018). The measured velocity fields would have a temporal resolution of 1 hr, which would be of great use for Stokes drift, since Stokes drift transport appears more sensitive to the temporal resolution of the data sets than the transport due to Ekman and geostrophic currents. This is due to Stokes drift being dependent on the wavefield, which responds quickly to changes in atmospheric conditions. In contrast, geostrophic balance responds to changes in conditions on timescales of days.

The modeled meridional microplastic distribution in the North Atlantic with the total currents is spread over nearly the entire basin, which does not agree with the clear peak in the observational meridional

distribution at around 40°W. Solely the Ekman currents do result in accumulation in two peaks around 40°W, but the addition of the Geostrophic currents leads to dispersal over a larger area. There are several possible reasons for the discrepancy, with the first being that relevant physical processes are not being included in the modeling. Complete inclusion of the Stokes drift could alleviate this, although it is also possible that submesoscale processes, which are not resolved with the 0.25° spatial resolution, are more crucial to microplastic transport than in the North Pacific. Another reason for the large discrepancy in the North Atlantic could be the uniform initial distribution. In a more realistic input distribution, continuous input of microplastic from the European coastlines could result in elevated concentrations being found further east than with a single uniform release. Finally, it must be considered that the observational record itself is scarce. Measurements were taken over a long period of time with various methods (albeit all with plankton nets) over a small fraction of the total surface area, where the samples are spatially nonuniformly spread with particularly low numbers in areas where the model discrepancy is largest. Aside from improved modeling, more measurements are therefore also required to be able to validate the model findings.

Martinez et al. (2009) first found that marine debris tends to accumulate in regions of low EKE, and for the North Pacific we find similar behavior. Maes et al. (2016) showed that the inclusion of mesoscale eddies results in more debris escaping the North Pacific accumulation zone. Since mesoscale eddies can transport mass, our initial hypothesis was that higher microplastic concentrations are observed in regions of low EKE since mesoscale eddies carry less microplastic away, which would allow high concentrations be maintained over time. In the North Pacific the region of low EKE coincides with the subtropical ocean gyre, and so Ekman currents can transport microplastic to the accumulation zone, and the low mesoscale eddy activity means that less microplastic is transported out of the accumulation zone by mesoscale eddies. In the North Pacific this hypothesis remains plausible, but we would expect to see similar patterns in the North Atlantic. Theoretical work has suggested that the EKE of subtropical gyres scales with the basin size (Spall, 2000), and therefore, it is possible that the smaller size of the North Atlantic basin leads to a less prominent role for mesoscale eddy activity. On the other hand, we see that the modeled North Atlantic accumulation zone has a larger zonal extent than in the North Pacific. This might be due to an absence of a local minimum in the EKE, with microplastic dispersion due to mesoscale eddy activity being constant throughout the subtropics. However, these remain hypotheses.

While we model transport as being purely two dimensional, biofouling of microplastic particles results in decreased buoyancy, which leads to sinking (Fazey & Ryan, 2016; Kooi et al., 2017). We also do not include vertical mixing of microplastic into the water column due to wind and waves (Kukulka et al., 2012; Reisser et al., 2015), which for high winds can be significant and lead to transport of microplastic by subsurface currents. Additionally, we do not consider microplastic removal processes, such as beaching and ingestion. Therefore, future microplastic modeling might consider three-dimensional flow fields with vertical microplastic dynamics and account for microplastic removal. Furthermore, in this paper we only compare our modeled distributions with observations in the North Pacific and North Atlantic due to insufficient sampling of the other ocean basins. There is therefore a great need for more microplastic sampling, especially outside the eastern North Pacific and the Western North Atlantic.

Acknowledgments
The code used for this work is distributed under the MIT license and can be found at the website (https://github.com/OceanParcels/SKIM-garbagepatchlocations). The v3.0 GlobCurrent data can be found at the website (http://www.ifremer.fr/opendap/cerdap1/globcurrent/v3.0/) and the WaveWatch III hindcast can be found at the website (ftp://ftp.ifremer.fr/ifremer/ww3/HINDCAST/GLOBAL/). This work was funded by the European Space Agency (ESA) through the Sea surface KInematics Multiscale monitoring (SKIM) Mission Science (SciSoc) Study (contract 4000124734/18/NL/CT/gp). D. W., P. D., and E. v. S. were supported through funding from the European Research Council (ERC) under the European Union's Horizon 2020 research and innovation programme (grant agreement 715386).

References

Ardhuin, F., Aksenov, Y., Benetazzo, A., Bertino, L., Brandt, P., Caubet, E., et al. (2018). Measuring currents, ice drift, and waves from space: The sea surface kinematics multiscale monitoring (SKIM) concept. *Ocean Science*, *14*(3), 337–354.

Bennett, V. C., & Mulligan, R. P. (2017). Evaluation of surface wind fields for prediction of directional ocean wave spectra during hurricane sandy. *Coastal Engineering*, *125*, 1–15.

Brach, L., Deixonne, P., Bernard, M. F., Durand, E., Desjean, M. C., Perez, E., et al. (2018). Anticyclonic eddies increase accumulation of microplastic in the North Atlantic subtropical gyre. *Marine Pollution Bulletin*, *126*, 191–96.

Breivik, Ø., & Allen, A. A. (2008). An operational search and rescue model for the Norwegian Sea and the North Sea. *Journal of Marine Systems*, *69*(1-2), 99–113.

Cancet, M., Griffin, D., Cahill, M., Chapron, B., Johannessen, J., & Donlon, C. (2019). Evaluation of globcurrent surface ocean current products: A case study in Australia. *Remote Sensing of Environment*, *220*, 71–93.

Chubarenko, I., Bagaev, A., Zobkov, M., & Esiukova, E. (2016). On some physical and dynamical properties of microplastic particles in marine environment. *Marine Pollution Bulletin*, *108*(1-2), 105–112.

Cózar, A., Echevarria, F., González-Gordillo, J. I., Irigoien, X., Ubeda, B., Hernandez-Leon, S., et al. (2014). Plastic debris in the open ocean. *Proceedings of the National Academy of Sciences*, *111*(28), 10239–10244.

Cózar, A., Martí, E., Duarte, C. M., García-De-Lomas, J., Sebille, E. Van, Ballatore, T. J., et al. (2017). The arctic ocean as a dead end for floating plastics in the North Atlantic branch of the thermohaline circulation. *Science Advances*, *3*(4), 1–8.

Dee, D. P., Uppala, S. M., Simmons, A. J., Berrisford, P., Poli, P., Kobayashi, S., et al. (2011). The ERA-Interim reanalysis: Configuration and performance of the data assimilation system. *Quarterly Journal of the Royal Meteorological Society*, *137*(656), 553–597.

Drivdal, M., Broström, G., & Christensen, K. H. (2014). Wave-induced mixing and transport of buoyant particles: Application to the Statfjord a oil spill. *Ocean Science*, *10*(6), 977–991.

Duhec, A. V, Jeanne, R. F., Maximenko, N., & Hafner, J. (2015). Composition and potential origin of marine debris stranded in the western Indian Ocean on remote Alphonse Island, Seychelles. *Marine Pollution Bulletin*, *96*(1-2), 76–86.

Eden, C., & Böning, C. (2002). Sources of eddy kinetic energy in the Labrador Sea. *Journal of Physical Oceanography*, *32*(12), 3346–3363.

Eriksen, M., Lebreton, L. C. M., Carson, H. S., Thiel, M., Moore, C. J., Borerro, J. C., et al. (2014). Plastic pollution in the world's oceans: More than 5 trillion plastic pieces weighing over 250,000 tons afloat at sea. *PLoS One*, *9*(12), 1–15.

Eriksen, M., Maximenko, N., Thiel, M., Cummins, A., Lattin, G., Wilson, S., et al. (2013). Plastic pollution in the South Pacific subtropical gyre. *Marine Pollution Bulletin*, *68*(1-2), 71–76.

Fan, Y., Lin, S.-J., Griffies, S. M., & Hemer, M. A. (2014). Simulated global swell and wind-sea climate and their responses to anthropogenic climate change at the end of the twenty-first century. *Journal of Climate*, *27*(10), 3516–3536.

Fazey, F. M., & Ryan, P. G. (2016). Biofouling on buoyant marine plastics: An experimental study into the effect of size on surface longevity. *Environmental Pollution*, *210*, 354–360.

Feng, H., Vandemark, D., Levin, J., & Wilkin, J. (2018). Examining the accuracy of globcurrent upper ocean velocity data products on the northwestern Atlantic shelf. *Remote Sensing*, *10*(8), 1205.

Fraser, C. I., Morrison, A. K., Hogg, A. McC, Macaya, E. C., van Sebille, E., Ryan, P. G., et al. (2018). Antarctica's ecological isolation will be broken by storm-driven dispersal and warming. *Nature Climate Change*, *8*, 704–708.

Froyland, G., Stuart, R. M., & van Sebille, E. (2014). How well-connected is the surface of the global ocean? *Chaos*, *24*, 3.

Galgani, F., Leaute, J., Moguedet, P., Souplet, A., Verin, Y., Carpentier, A., et al. (2000). Litter on the sea floor along European coasts. *Marine Pollution Bulletin*, *40*(6), 516–527.

Hart-Davis, M. G., Backeberg, B. C., Halo, I., van Sebille, E., & Johannessen, J. A. (2018). Assessing the accuracy of satellite derived ocean currents by comparing observed and virtual buoys in the greater Agulhas region. *Remote Sensing of Environment*, *216*, 735–746.

Henderson, J. R. (2001). A pre-and post-MARPOL annex V summary of Hawaiian monk seal entanglements and marine debris accumulation in the northwestern Hawaiian islands, 1982–1998. *Marine Pollution Bulletin*, *42*(7), 584–589.

Jambeck, J. R., Geyer, R., Wilcox, C., Siegler, T. R., Perryman, M., Andrady, A., et al. (2015). Plastic waste inputs from land into the ocean. *Science*, *347*(6223), 768–771.

Kooi, M., van Nes, E. H., Scheffer, M., & Koelmans, A. A. (2017). Ups and downs in the ocean: Effects of biofouling on vertical transport of microplastics. *Environmental Science & Technology*, *51*(14), 7963–7971.

Kubota, M. (1994). A mechanism for the accumulation of floating marine debris north of Hawaii. *Journal of Physical Oceanography*, *24*(5), 1059–1064.

Kubota, M., Takayama, K., & Namimoto, D. (2005). Pleading for the use of biodegradable polymers in favor of marine environments and to avoid an asbestos-like problem for the future. *Applied Microbiology and Biotechnology*, *67*(4), 469–476.

Kukulka, T., Proskurowski, G., Morét-Ferguson, S., Meyer, D. W., & Law, K. L. (2012). The effect of wind mixing on the vertical distribution of buoyant plastic debris. *Geophysical Research Letters*, *39*, L07601. https://doi.org/10.1029/2012GL051116

Lacorata, G., Corrado, R., Falcini, F., & Santoleri, R. (2019). Fsle analysis and validation of Lagrangian simulations based on satellite-derived globcurrent velocity data. *Remote Sensing of Environment*, *221*, 136–143.

Lange, M., & Van Sebille, E. (2017). Parcels v0.9: Prototyping a Lagrangian ocean analysis frameworkfor the petascale age. *Geoscientific Model Development Discussions*, *10*, 4175–4186.

Law, K. L., Moret-Ferguson, S. E., Goodwin, D. S., Zettler, E. R., Deforce, E., Kukulka, T., & Proskurowski, G. (2014). Distribution of surface plastic debris in the eastern Pacific Ocean from an 11-year data set. *Environmental Science & Technology*, *48*(9), 4732–4738.

Law, K. L., Moret-Ferguson, S., Maximenko, N. A., Proskurowski, G., Peacock, E. E., Hafner, J., & Reddy, C. M. (2010). Plastic accumulation in the North Atlantic subtropical gyre. *Science*, *329*(5996), 1185–1188.

Lebreton, L. C.-M., Greer, S. D., & Borrero, J. C. (2012). Numerical modelling of floating debris in the world's oceans. *Marine Pollution Bulletin*, *64*(3), 653–661.

Lebreton, L. C.-M, Slat, B., Ferrari, F., Sainte-Rose, B., Aitken, J., Marthouse, R., et al. (2018). Evidence that the great Pacific garbage patch is rapidly accumulating plastic. *Scientific Reports*, *8*(1).

Lebreton, L. C.-M., Van Der Zwet, J., Damsteeg, J.-W., Slat, B., Andrady, A., & Reisser, J. (2017). River plastic emissions to the world's oceans. *Nature Communications*, *8*, 15611.

Maes, C., Blanke, B., & Martinez, E. (2016). Origin and fate of surface drift in the oceanic convergence zones of the eastern Pacific. *Geophysical Research Letters*, *43*, 3398–3405. https://doi.org/10.1002/2016GL068217

Martinez, E., Maamaatuaiahutapu, K., & Taillandier, V. (2009). Floating marine debris surface drift: Convergence and accumulation toward the south Pacific subtropical gyre. *Marine Pollution Bulletin*, *58*(9), 1347–1355.

Mascarenhas, R., Santos, R., & Zeppelini, D. (2004). Plastic debris ingestion by sea turtle in Paraíba, Brazil. *Marine Pollution Bulletin*, *49*(4), 354–355.

Maximenko, N., Hafner, J., & Niiler, P. (2012). Pathways of marine debris derived from trajectories of Lagrangian drifters. *Marine Pollution Bulletin*, *65*(1-3), 51–62.

Molnar, J. L., Gamboa, R. L., Revenga, C., & Spalding, M. D. (2008). Assessing the global threat of invasive species to marine biodiversity. *Frontiers in Ecology and the Environment*, *6*(9), 485–492.

Montiel, F., Squire, V., Doble, M., Thomson, J., & Wadhams, P. (2018). Attenuation and directional spreading of ocean waves during a storm event in the autumn Beaufort sea marginal ice zone. *Journal of Geophysical Research: Oceans*, *123*, 5912–5932. https://doi.org/10.1029/2018JC013763

Morét-Ferguson, S., Law, K. L., Proskurowski, G., Murphy, E. K., Peacock, E. E., & Reddy, C. M. (2010). The size, mass, and composition of plastic debris in the western North Atlantic ocean. *Marine Pollution Bulletin*, *60*(10), 1873–1878.

Pieper, C., Ventura, M. A., Martins, A., & Cunha, R. T. (2015). Beach debris in the azores (NE Atlantic): Faial island as a first case study. *Marine pollution bulletin*, *101*(2), 575–582.

Prasetya, G., Black, K., De Lange, W., Borrero, J., & Healy, T. (2011). Debris dispersal modeling for the Great Sumatra Tsunamis on Banda Aceh and surrounding waters. *Natural Hazards*, *60*(3), 1167–188.

Rascle, N., & Ardhuin, F. (2013). A global wave parameter database for geophysical applications. Part 2: Model validation with improved source term parameterization. *Ocean Modelling*, *70*, 174–188.

Reisser, J., Slat, B., Noble, K., Plessis, K. Du, Epp, M., Proietti, M., et al. (2015). The vertical distribution of buoyant plastics at sea: An observational study in the North Atlantic gyre. *Biogeosciences*, *12*(4), 1249–256.

Rio, M.-H., Mulet, S., & Picot, N. (2014). Beyond GOCE for the ocean circulation estimate: Synergetic use of altimetry, gravimetry, and in situ data provides new insight into geostrophic and Ekman currents. *Geophysical Research Letters*, *41*, 8918–925. https://doi.org/10.1002/2014GL061773

Rio, M.-H., Piollé, J.-F., Johannessen, J. H., & Donlan, C. (2015). Globcurrent: Product format and content: ESA.

Saha, S., Moorthi, S., Wu, X., Wang, J., Nadiga, S., Tripp, P., et al. (2011). NCEP Climate Forecast System Version 2 (CFSv2) 6-hourly Products. Boulder, CO: Research Data Archive at the National Center for Atmospheric Research, Computational and Information Systems Laboratory. https://doi.org/10.5065/D61C1TXF

Spall, M. A. (2000). Generation of strong mesoscale eddies by weak ocean gyres. *Journal of marine research*, *58*(1), 97–116.

Tamura, H., Miyazawa, Y., & Oey, L.-Y. (2012). The stokes drift and wave induced-mass flux in the North Pacific. *Journal of Geophysical Research*, *117*, C08021. https://doi.org/10.1029/2012JC008113

Thompson, R. C., Olsen, Y., Mitchell, R. P., Davis, A., Rowland, S. J., John, A. W. G., et al. (2004). Lost at sea: Where is all the plastic? *Science*, *304*(5672), 838.

Tolman, H. L. (1997). *User manual and system documentation of wavewatch-III version 1.15*. Washington, DC: US Department of Commerce, National Oceanic and Atmospheric Administration, National Weather Service, National Centers for Environmental Prediction.

Tolman, H. L. (2009). User manual and system documentation of wavewatch III TM version 3.14. *Technical Note, MMAB Contribution*, *276*, 220.

Trinanes, J. A., Olascoaga, J. M., Goni, G. J., Maximenko, N. A., Griffin, D. A., & Hafner, J. (2016). Analysis of flight MH370 potential debris trajectories using ocean observations and numerical model results. *Journal of Operational Oceanography*, *9*(2), 126–138.

Van Cauwenberghe, L., Vanreusel, A., Mees, J., & Janssen, C. R. (2013). Microplastic pollution in deep-sea sediments. *Environmental Pollution*, *182*, 495–499.

van Franeker, J. A., & Law, K. L. (2015). Seabirds, gyres and global trends in plastic pollution. *Environmental Pollution*, *203*, 89–96.

van Sebille, E., England, M. H., & Froyland, G. (2012). Origin, dynamics and evolution of ocean garbage patches from observed surface drifters. *Environmental Research Letters*, *7*(4), 1–6.

van Sebille, E., Wilcox, C., Lebreton, L., Maximenko, N., Hardesty, B. D., Van Franeker, J. A., et al. (2015). A global inventory of small floating plastic debris. *Environmental Research Letters*, *10*(12), 1–11.

van den Bremer, T., & Breivik, Ø. (2018). Stokes drift. *Philosophical Transactions of the Royal Society A*, *376*(2111), 20170104.

Webb, A., & Fox-Kemper, B. (2015). Impacts of wave spreading and multidirectional waves on estimating stokes drift. *Ocean Modelling*, *96*, 49–64.

Young, A. M., & Elliott, J. A. (2016). Characterization of microplastic and mesoplastic debris in sediments from Kamilo beach and Kahuku beach, Hawai'i. *Marine pollution bulletin*, *113*(1-2), 477–482.